

RESEARCH ARTICLE

Temporal and spatial variation of the transitional climate zone in summer during 1961–2018

Qiulin Wang^{1,2}  | Lin Wang³  | Gang Huang^{1,2}  | Jinling Piao⁴ |
Chakrit Chotamonsak^{5,6}

¹State Key Laboratory of Numerical Modeling for Atmospheric Sciences and Geophysical Fluid Dynamics, Institute of Atmospheric Physics, Chinese Academy of Sciences, Beijing, China

²College of Earth and Planetary Sciences, University of Chinese Academy of Sciences, Beijing, China

³CAS Key Laboratory of Regional Climate-Environment for Temperate East Asia, Institute of Atmospheric Physics, Chinese Academy of Sciences, Beijing, China

⁴Center for Monsoon System Research, Institute of Atmospheric Physics, Chinese Academy of Sciences, Beijing, China

⁵Regional Center for Climate and Environmental Studies Faculty of Social Sciences, Chiang Mai University, Chiang Mai, Thailand

⁶Department of Geography, Faculties of Social Sciences, Chiang Mai University, Chiang Mai, Thailand

Correspondence

Lin Wang, Institute of Atmospheric Physics, Chinese Academy of Sciences, Beijing 100029, China.
Email: linwang@mail.iap.ac.cn

Funding information

National Natural Science Foundation of China, Grant/Award Numbers: 41875115, 41961144016, 41831175, 41530425; the Key Deployment Project of Centre for Ocean Mega-Research of Science, Chinese Academy of Science, Grant/Award Number: COMS2019Q03

Abstract

The transitional climate zone (TCZ) over East Asia is an interface area between monsoon circulation and westerly circulation, making it highly susceptible to natural disasters and climate change. This study explores the spatial–temporal variation of the summer (May–September) TCZ during 1961–2018 and its response to monsoon rainy season. The summer Aridity Index (AI) instead of annual amount is used to recognize summer TCZ, with similar domain produced. However, differing from the annual total, the summer evaporation remains stable during the whole period, despite global warming. Hence, the summer TCZ has experienced little significant long-term trends toward wetter or drier, since it is predominantly driven by precipitation that shows no clear tendency. The EOF decomposition reveals three key patterns accounting for 58.2% of the total variance: spatially uniform, south–north dipole and meridional tripole, which shows the complexity of spatial-temporal variation in TCZ. TCZ is characterized by interdecadal mutations and periodical oscillations of 3 or 8 years. There exist remarkable 3 years interannual periods, with the greatest contribution stemming from the south-central part of TCZ. In comparison, the northeast part exhibits a significant interdecadal band of about 8 years, which promotes the regime shift from wet to dry in the late 1990s over TCZ. Furthermore, the onset, retreat, and duration of the rainy season of TCZ in response to summer monsoon are examined, based on EEMD filtered 4 mm/day precipitation. All three indicators are subjected to strong interannual dispersion, without any significant overall trends. Only the retreat date of the western part of TCZ (100–110°E) is significantly correlated with the onset date. Dry-wet condition in TCZ is more closely associated with the duration length of the monsoon influence. And we also notice that the westmost part of TCZ shows a greater sensitivity to monsoon activity than the east part.

KEYWORDS

aridity index, monsoon rainy season, precipitation, transitional climate zone

1 | INTRODUCTION

The transitional climate zone (TCZ) over East Asia is an interface area between humid and arid regions and harbours semi-arid environment (Fu, 1992). It geographically stretches from the eastern fringe of Tibetan Plateau to Northeast China. This intercross zone is featured by large gradients of climate and biome, the interaction between the East Asian summer monsoon and the mid-latitude westerly winds (Qian *et al.*, 2009). As the marginal area affected by East Asia summer monsoon (EASM), TCZ is also known as monsoon transitional zone. Although TCZ is only a narrow belt, its responses to natural disturbance and human-driven global change exert fundamental climatic and ecological significances. This region, also known as a farming-pastoral ecotone (FPE), is mainly covered by grassland and open shrubland, which indicates the vegetation there is unstable and sensitive to climate fluctuations (Ou and Qian, 2006). Lu and Jia (2013) reveal the FPE extent greatly fluctuated in accordance with the variability of precipitation associated with changing East Asia monsoon in the past 25 years. In addition to fragile ecology, TCZ is intensively sensitive to climate change. With the pace of global warming, the most significant aridification trend occurred in this region in the last century (Huang *et al.*, 2017). Moreover, complex geologic environment and climatic condition make TCZ highly susceptible to natural disasters like droughts, floods and hailstorms (Shi *et al.*, 1994), which in turn poses great threats to human society. Therefore, getting better understanding of climate changes in TCZ is quite critical and essential, and becomes one of the frontiers in climate change research.

There are plenty of studies on climate change in monsoon area and its possible mechanisms (Wang *et al.*, 2013; Li *et al.*, 2014; Wang *et al.*, 2014; Li and Zhou, 2015). However, the studies that specifically deal with TCZ are still in the early stage (Chen *et al.*, 2019). Chen *et al.* (2018) shows that there is a 200–700 km fluctuation range of the interannual EASM northern boundaries around the locations of the climatological northern boundary, in terms of 2 mm/day precipitation isoline. It is noticed that the TCZ has experienced the largest warming over East Asia during the past 100 years (Huang *et al.*, 2012a; Huang *et al.*, 2012b; Li *et al.*, 2015a; Li *et al.*, 2015b; Huang *et al.*, 2019). Meanwhile, the most significant aridity trend and expansion occurred over this region, no matter which drought index is used (Wang *et al.*, 2017; Chen and Sun, 2015; Zhang and Zhou, 2015). Further, Wang *et al.* (2017) identified the separate effects of precipitation and evaporation on the position of TCZ based on Aridity Index (AI) which is defined by annual total precipitation divided by potential evaporation. Their

results showed that the interannual fluctuation of both fringes of TCZ is mainly controlled by precipitation variation, while the long-term trend owes much more to increasing evaporation. Piao *et al.* (2017) detected an interdecadal change that occurred in the 1990s after which the drought is exacerbated, over the Asian inland plateau that is part of the TCZ. The possible cause is associated with summer warming sea surface temperature in the North Atlantic exciting a teleconnection pattern over Eurasia. A similar conclusion is also achieved by Zhao *et al.* (2019, 2020). Wang and Li (2011) found a negative correlation between surface sensible heat flux in the arid region of northwestern China and the northern boundary of the East Asian summer monsoon, via the teleconnection wave train structure of the geopotential height field at 500 hPa.

All these studies above contributed to a better understanding of TCZ. However, there are still key issues to be addressed. As noted before, firstly, we know the significant aridification occurred in TCZ over East Asia, largely induced by enhanced evaporation. However, whether the summer TCZ also exhibit a long-term drying trend? Second, previous studies treated the TCZ as a whole or select a subregion. In fact, the drought variation throughout China, even just Northern China, is quite inhomogeneous (Li *et al.*, 2015a; Li *et al.*, 2015b). The interannual diversity of EASM brings different impacts on different subregions, so that it is necessary to unravel the dominant structure of TCZ and the leading periodicities. Third, the studies about how the advance and retreat of the EASM influence the rainy season of TCZ in summer is much less. Thus, it is of great importance to reveal the onset, retreat date and duration of TCZ rainy season long with their variability, and highlight which is mostly responsible for the dry-wet variation in TCZ. This article first focuses on temporal and spatial variation characteristics of the transition zone, and then we partition TCZ based on REOF analysis and study the interannual and decadal variations in its subregions. Finally, we attempt to identify the date when monsoon rainy season begins and ends, and how long it lasts in different longitude range of TCZ, as well as their correlation with the climate viability in TCZ.

This article is organized as follows. Section 2 describes data sources, the definition of relevant physical quantities and their calculation method. Section 3 provides an overview of the climatology and linear trend of TCZ. In Section 4, we discuss the spatial patterns of TCZ according to EOF results, and then partition TCZ into three subareas based on REOF to discuss the changes in TCZ and all three subregions. Section 5 elaborates when monsoon rainy season begins and ends, as well as its duration, and how TCZ response to them. Section 6 provides a summary of this article.

2 | DATA AND METHOD

2.1 | Data

The gridded daily precipitation and surface air maximum/minimum temperature datasets from 1961 to 2018 used in this study are retrieved from National Meteorological Information Center, with a spatial resolution of $0.5^\circ \times 0.5^\circ$. These datasets are compiled by interpolation from observations of more than 2000 surface meteorological stations in China. Due to the increase of the data of the setting station with better interpolation parameters and the selection of the appropriate spatial resolution, the datasets provided error small and high resolution (Xu *et al.*, 2019). The monthly datasets including wind fields, geopotential height and precipitable water applied in this study is the Japanese 55-year Reanalysis (JRA-55), the second global reanalysis constructed by the Japan Meteorological Agency (JMA; Kobayashi *et al.*, 2015; Harada *et al.*, 2016), with a resolution of $1.25^\circ \times 1.25^\circ$.

2.2 | Aridity index

AI refers to the ratio of annual precipitation (PRE) to annual potential evapotranspiration (PET), which indicates the degree of water deficiency in a given region. Drylands are categorized as hyper-arid ($AI \leq 0.05$), arid ($0.05 \leq AI \leq 0.2$), semi-arid ($0.2 \leq AI \leq 0.5$) and dry sub-humid ($0.5 \leq AI \leq 0.65$) regions, while AI in humid region is greater than 0.65 (Huang *et al.*, 2017; Wang *et al.*, 2017; Huang *et al.*, 2019). The TCZ is the area where AI is greater than 0.2 and less than 0.65. Since we mainly focus on the dry and wet condition of TCZ during summer and the influence of EASM, summer precipitation and evaporation were used to calculate the index instead of annual amounts. The summer season in this study is taken to include May, June, July, August and September. In order to avoid confusion, we design an index called summer AI (SM_AI):

$$SM_AI(\text{Summer Aridity Index}) = SM_PRE / SM_PET \quad (1)$$

SM_PRE and SM_PET refer to the cumulative value of daily PRE and PET in summer. The daily PET used in here is calculated by Hargreaves and Samani method (Hargreaves and Samani, 1985), which only need surface air temperature datasets:

$$PET = 0.0023 \cdot R_a \cdot \frac{1}{\lambda} (T_{\max} - T_{\min})^{0.5} (T_{\text{mean}} + 17.8) \quad (2)$$

$$T_{\text{mean}} = \frac{1}{2} (T_{\max} + T_{\min}) \quad (3)$$

Where $\lambda = 2.45 \text{ MJ} \cdot \text{kg}^{-1}$; R_a is extraterrestrial radiation, unit: $\text{MJ} \cdot \text{m}^{-2} \cdot \text{d}^{-1}$; T_{\max} and T_{\min} are maximum and minimum surface air temperature.

We also use 0.65 and 0.2 as the front and rear limits of the transitional zone. As shown in Figure 1, TCZ is mainly located in the north of China to the east of 100°E , oriented from Southwest China to Northeast China. Although both two boundary lines fluctuate greatly from year to year, the south fringe has a stronger amplitude than the north one. It is worth noting that the south boundary exhibits a dry “tongue” extending to the south-east part of Northeast China ($120\text{--}125^\circ\text{E}$).

2.3 | Definition of EASM influence time

A wide variety of definitions exist in the definition for the northernmost location of EASM (Zeng and Lu, 2004; Qian and Qin, 2007; Fei *et al.*, 2009; Qian *et al.*, 2009). Based on previous studies, precipitation of 4 mm/day is used in this article as a criterion to describe the north front position of monsoon activity (Qian *et al.*, 2007). Monsoon rainfall in TCZ begins with daily precipitation reaching 4 mm/day (MRO, units: Julian Day, JD) and ends with the last time precipitation (MRR, units: Julian Day, JD) reaching 4 mm/day. However, using the raw 4 mm/day isoline is not feasible to detect the influence time of EASM, due to the presence of high-frequency oscillation. In order to address this issue, the ensemble empirical mode decomposition (EEMD) method was used to filter daily precipitation sequences with

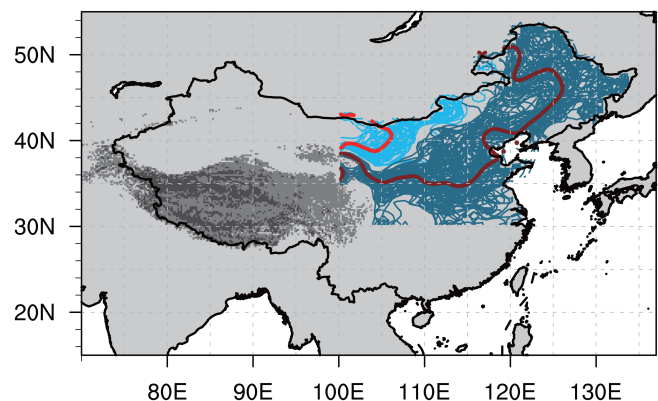


FIGURE 1 Front (light blue lines) and rear (deep blue lines) edges of TCZ for each year during 1961–2018 and climatologic positions (thick red line) [Colour figure can be viewed at wileyonlinelibrary.com]

intraseasonal oscillation and longer time scale components (SLC) retained. The steps to extract SLC by the EEMD method are as follows (Qian *et al.*, 2011):

1. Decompose the daily precipitation series into Intrinsic Mode Functions (IMFs) using the EMD approach with added white noise of 0.3 and run an ensemble of 1,000 decompositions. After that, the ensemble means of the corresponding IMFs of the decompositions are obtained.
2. Combined the fifth component through the last components as SLC. Note that the periods of all the components used are longer than a month, so an intraseasonal oscillation can be included in the reconstructed series (Wang and LinHo, 2002).

In the following, MRO, MRR and MRD stand for the onset, retreat, and duration of the rainy season of TCZ in response to summer monsoon. Specifically, MRO of TCZ is the time when the EEMD filtered precipitation sequence in the corresponding southern boundary reaches the threshold of 4 mm/day for the first time from May to September, while MRR for the last time reaching the threshold. Difference of the onset and retreat dates (duration = retreat - onset + 1) is MRD. An example of EEMD procedure and corresponding MRO, MRR and MRD identification is shown in Figure 2. It shows MRO, MRR and MRD of the north region with longitude range of 110–115°E, 36°N in 1971.

3 | CLIMATOLOGY AND LINEAR TREND

According to Figure 3a, it was very distinguished that summer precipitation was unevenly distributed in China.

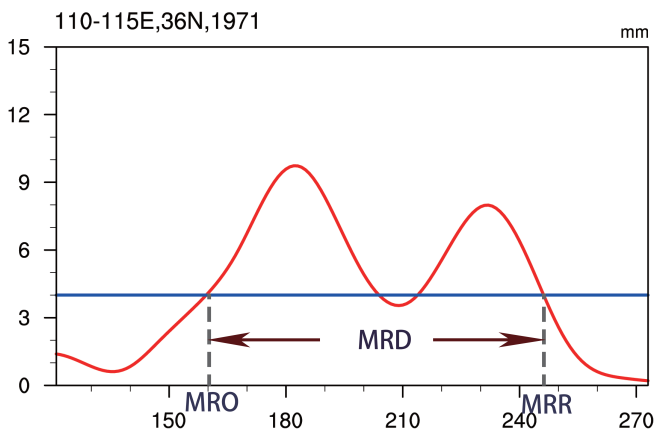


FIGURE 2 The definition of MRO, MRR and MRD of one segment of the southern boundary of TCZ (110–115E, 36N) in 1971 [Colour figure can be viewed at wileyonlinelibrary.com]

It generally decreases from south to north and from the coast to the interior, with the lowest precipitation located in the northwest. The summer rainfall in TCZ is about 150–450 mm, with a large spatial gradient. The spatial diversity of summer PET in China (Figure 3b) is not as obvious as the precipitation. In TCZ, summer PET is 600–750 mm, greater than PRE, which indicates that the atmospheric water demand is greater than the supply. The distribution of SM_AI (Figure 3c) in China is similar to PRE, and also features a large spatial gradient in TCZ.

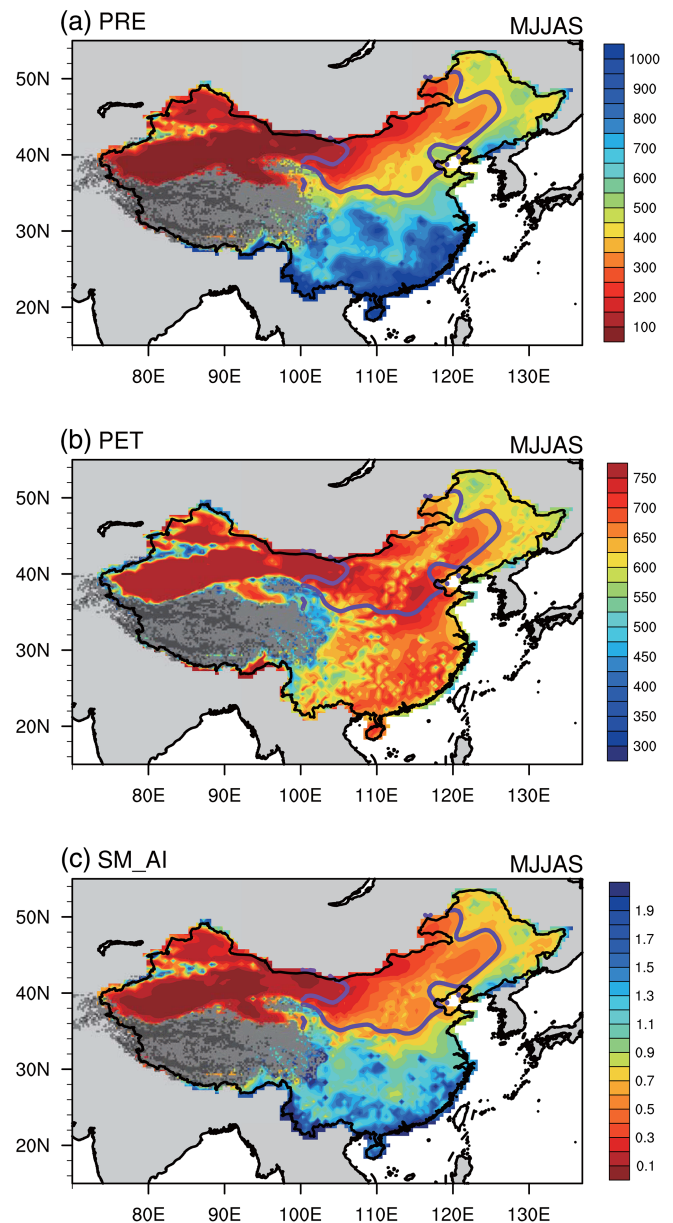


FIGURE 3 Long-term mean of summer total precipitation (a, unit: mm), PET (b, unit: mm), and SM_AI (c, unit: year⁻¹) during 1961–2018. Thick purple line encloses the climatological TCZ domain [Colour figure can be viewed at wileyonlinelibrary.com]

The variation of wet-dry climate in summer in China is complicated during 1961–2018. As shown in Figure 4, the linear trend of summer precipitation, potential evapotranspiration and SM_AI were quite heterogeneous in China during 1961–2018. A wetter trend is observed in most parts of Southeast China, as well as in the north of Inner Mongolia and part of Heilongjiang Province, while the Southwest China and most of Northeast China have experienced drying tendency. With regard to TCZ region, the linear trend reveals a “drier in the northeast and

wetter in the southwest” pattern. During the past half-century, summer precipitation decreased over the northeast and the southern flank of TCZ whereas increased in the northwest in China, which is generally consistent with the results of previous studies (Xu *et al.*, 2015). The change of summer PET is quite different from summer rainfall. The linear trend of PET in TCZ is negative in the south of Hebei and the northeast “dry tongue” area, while a significant increase is found in the center area of TCZ. On the whole, the magnitude of potential evaporation change is less than that of precipitation change. However, it is important to note that the trends are not statistically significant at the 10% significance level in most parts of TCZ. As reported in previous study, the annual AI witnesses a uniform significant downward tendency as a consequence of enhancing PET (Wang *et al.*, 2017). That is, the summer trend is rather weak and heterogeneous, compared with annual totals. The most likely cause maybe that the warming trend is particularly enhanced, in the boreal cold season (November to March) over semi-arid regions (Huang *et al.*, 2012a), so the PET trend in TCZ during summer time is not as obvious as annual trend.

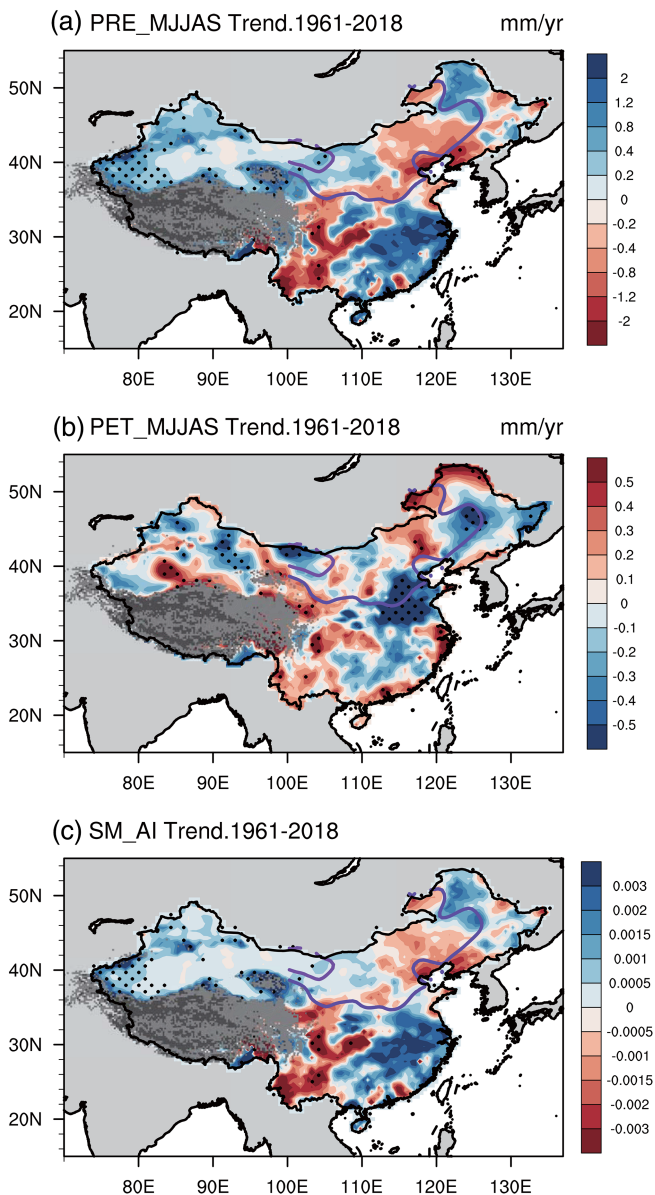


FIGURE 4 Trend maps of summer PRE (a, mm year^{-1}), PET (b, mm year^{-1}), SM_AI (c) from May to summer during 1961–2018. Dots indicate the regions where the linear trend is statistically significant at .1 level. Thick purple line encloses the climatological TCZ domain [Colour figure can be viewed at wileyonlinelibrary.com]

4 | SPATIAL AND TEMPORAL PATTERNS OF ARIDITY VARIABILITY OVER TCZ DURING 1961–2018

4.1 | EOF analysis of TCZ

In order to separate dominant spatial and temporal patterns, EOF analysis is applied to summer AI in TCZ during 1961–2018. Figure 5 displays the first three EOF modes and corresponding normalized principal components of SM_AI anomaly in TCZ during 1961–2018. The first three modes account for 32.4, 15.9 and 9.9% of the total variance, respectively, and can be isolated from other modes based on the criteria by North *et al.* (1982). The cumulative variance contribution is 58.2%. FFT filter is performed to abstract the interannual components of the corresponding PCs which explains majority of the variance (72.3, 75.4 and 66.7%), as well as the remaining interdecadal components. The first mode EOF1 (Figure 5a) shows a uniform anomalous pattern, which indicates that the whole transition zone mainly presents coherent changes, and high loadings are detected in the south part of TCZ. The corresponding time coefficient PC1 has great interannual and interdecadal fluctuation (Figure 5b). In the late 1990s, PC1 dropped rapidly, implying a drying process over TCZ. It was not until 2010 that the PC1 began to recover and the TCZ is becoming

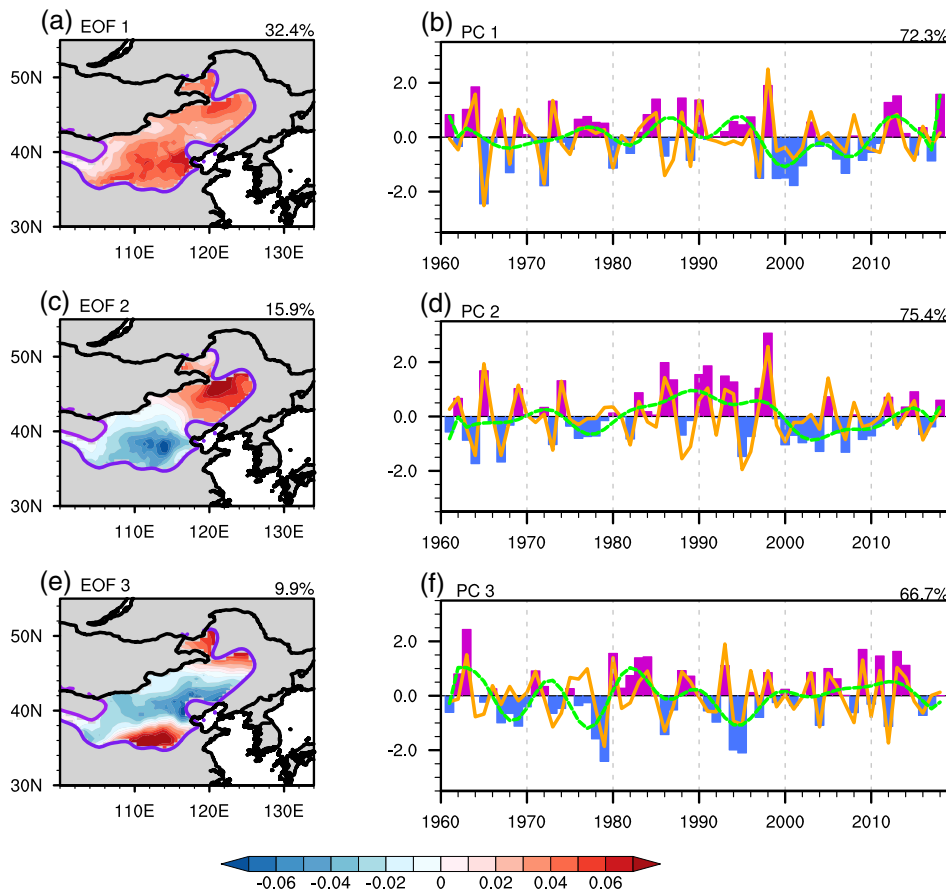


FIGURE 5 (a), (c) and (e) the first three modes (EOF1, EOF2 and EOF3) and (b), (d) and (f) corresponding standardized time coefficients (PC1, PC2 and PC3) of EOF analysis on SM_AI anomaly in TCZ during 1961–2011. The contributions of the first three modes to the total variance account for 32.4, 15.9 and 9.9%. The orange solid lines are interannual components of PCs, explaining 72.3, 75.4 and 66.7% of the variance of corresponding PCs, respectively. The green dashed lines are remaining decadal components [Colour figure can be viewed at wileyonlinelibrary.com]

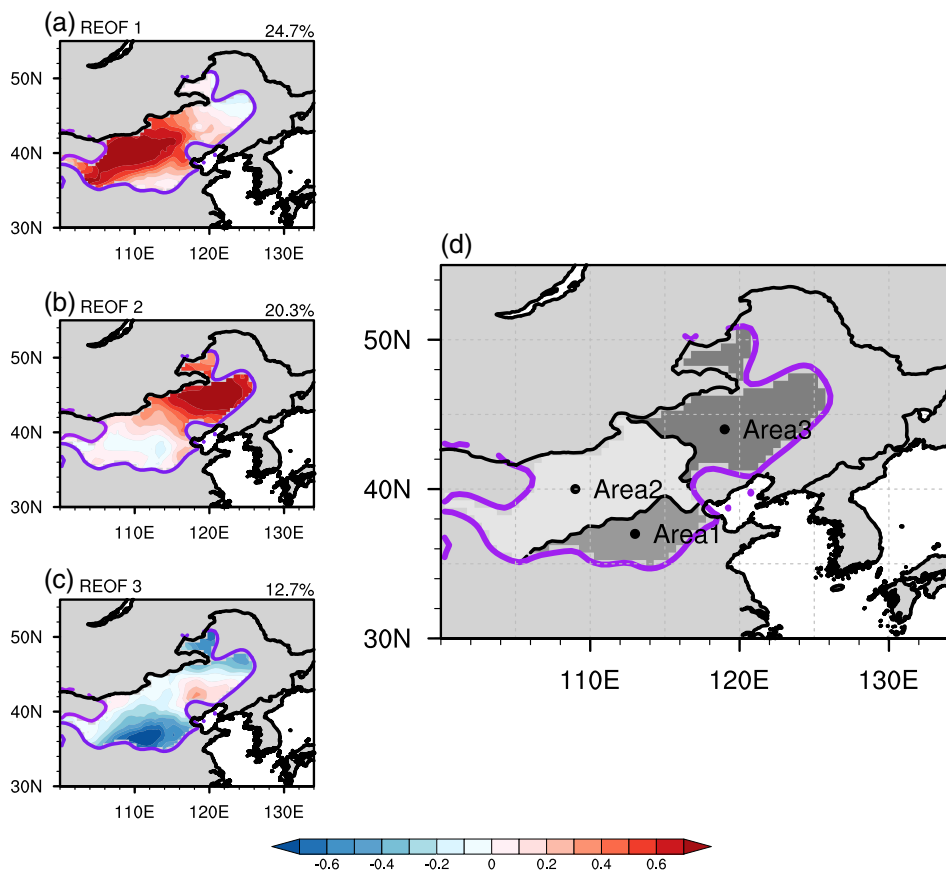


FIGURE 6 (a–c) the first three modes (REOF1, REOF2 and REOF3) of REOF analysis on SM_AI anomaly in TCZ during 1961–2011 and (d) three sub-regions (Area 1–3) identified by REOF analysis. The contributions of the first three modes to the total variance account for 24.7, 20.3 and 12.7%, respectively [Colour figure can be viewed at wileyonlinelibrary.com]

wetter thereafter. The EOF2 (Figure 5c) is characterized by southwest-northeast out-of-phase pattern. From the mid-1980s to the late 1990s, the northeast was generally wetter and the southwest drier. However, the situation was reversed by the early 2000s, with the northeast drier and the southwest wetter. By synthesizing the first two modes, we can infer that the northeast part of TCZ experienced a significant drying process during the late 1990s to 2000. The third mode revealed a “- + -” meridional tripole structure. From the early 1990s to the early 2000s, the southernmost and northernmost parts of TCZ were

drier with the central being wetter, while the opposite is true by around 2010.

4.2 | Division of TCZ based on REOF and dry-wet variability in subregions

According to EOF analysis results and long-term linear trend, the wet-dry climate variability in TCZ is complex and different part of TCZ is subject to different characteristics. The eigenvectors from EOF analysis reveal the

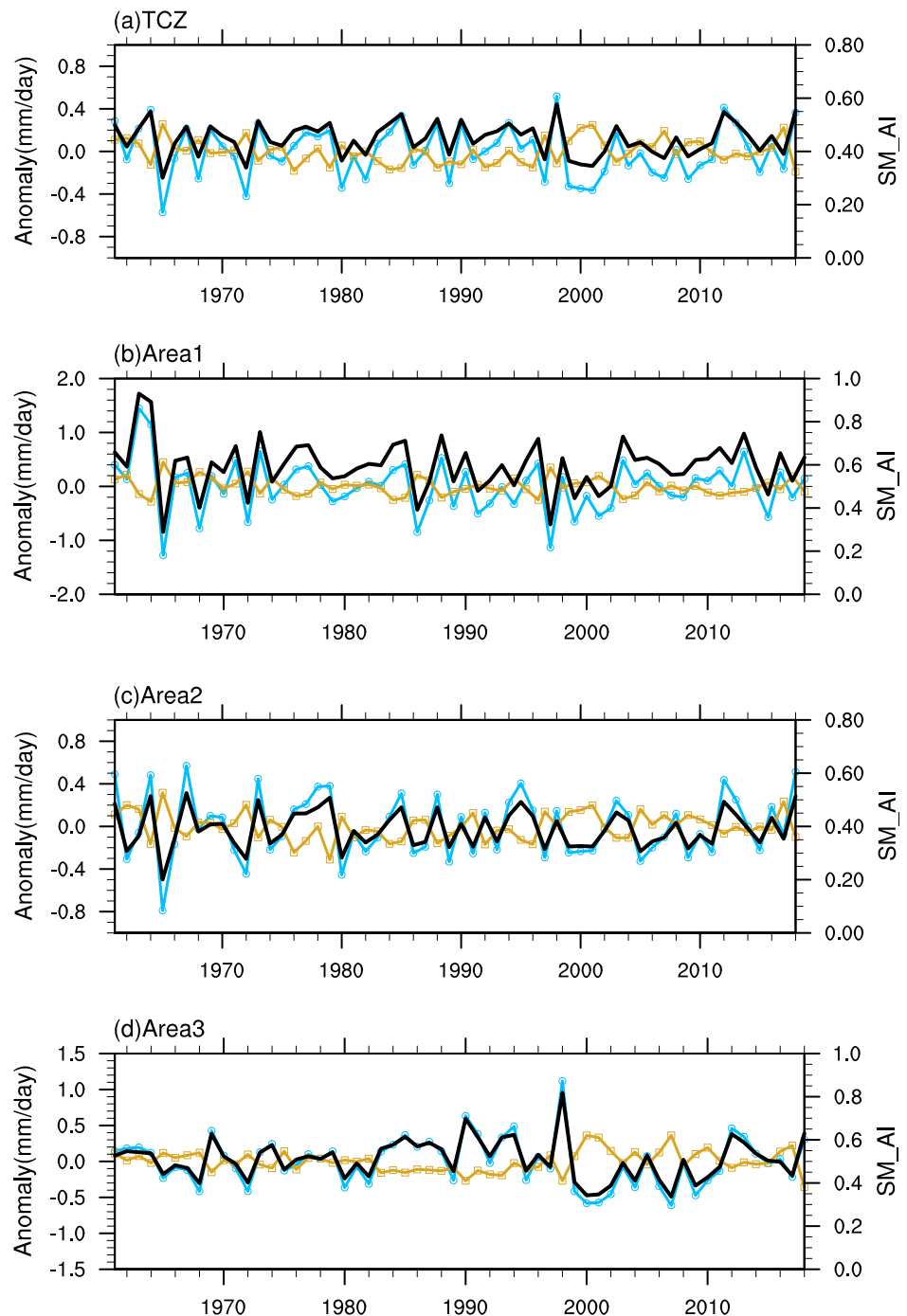


FIGURE 7 Time series of summer PET (yellow line with square markers) and PRE (blue line with circle markers) anomalies as well as SM_AI (thick solid line) for the whole TCZ (a) and its three subregions during 1961–2018 (b–d) [Colour figure can be viewed at wileyonlinelibrary.com]

structure of the whole region of climate variable field to the greatest extent, and the principle components show variation of the corresponding EOF patterns, but they cannot demonstrate the variation characteristics in different areas specifically. To better explore the climate in TCZ, it is necessary to make a reasonable division of the entire TCZ. To this end, the rotated empirical orthogonal function (REOF) method, a widely used clustering algorithm to objectively capture realistic spatial information, is employed in the current study to identify the homogeneous regions regarding standardized SM_AI (Figure 6). Three subregions (Figure 6d) are delimited based on the anomalous center of the first three REOFs: Area1 (the south region), Area2 (the northwest region), Area3 (the northeast region).

Figure 7 depicts the area-averaged time series of summer PRE, PET anomalies, and SM_AI over the TCZ and its three subregions from 1961 to 2018. In all three subregions, the amplitude of summer rainfall fluctuation is greater than PET, and dominantly drives SM_AI changes. The strongest interannual fluctuation happens in the south subregion (Area 1), while the northwest region is quite steady. We also notice that there is a dramatic shift to drier condition around the late 1990s.

Change-point detection algorithms and spectral analysis are applied for better understanding the characteristics of climatic variation (Qian *et al.*, 2007; Li and Zhou, 2014; Wang *et al.*, 2014). In this study, moving *t*-test (MTT) with a 9-year window was applied to detect the abrupt change point of the decadal variation in TCZ and three subareas (Figure 8). Due to the combined effect of PRE and PET, there appears to be a significant wet-to-dry shift in 1998 and an opposite abrupt change around 2007 (Figure 8a), with regard to the entire TCZ. Out of the three subregions, the interdecadal change is strongest in Area 3, which is likely to govern the behaviour of the entire TCZ. In addition, apart from shifts in 1998 and 2007, another abrupt change is recorded in 1982 over Area 3. Contrasting to Area3, it is found interdecadal signals are much weaker in Area 1 and Area 2. However, in spite of great interannual fluctuation of SM_AI, only one abrupt point is identified in Area1, which barely passes significance test at the level of .05 and implies a wetter process in 2002 (Figure 8b). Meanwhile, SM_AI and summer precipitation in the northwest area (Area 2) was relatively steady with no abrupt detected (Figure 8c).

As shown in Figure 9, wavelet analysis (Morlet wavelet) decomposes time coefficients series into time and frequency space showing periodicities at different frequency bands (Torrence and Compo, 1998). The ribbon indicates the magnitude of the wavelet coherence at a specific time and frequency (i.e., the period). Significant intervals of interannual variability come and go intermittently in

TCZ and its three subregions. There are 3 and 8-year fluctuations in TCZ with a possible strong 28-year decadal oscillation background field outside of the cone of influence (Figure 9a). In accordance with these oscillations, the dry and wet condition experienced alternations of relatively dry and wet periods. In the late 1990s, there is an almost vertical zero isoline with a change from positive to negative in corresponding real part spectrum, indicating a pronounced drying progress (Figure 9b). Dominant variation period of SM_AI in Area1 is 3-year interannual oscillation. And its real part spectrum reflects a prominent drop of SM_AI around 1964 as well as a rise around 2002 (Figure 9c, d). In addition to a 3-yr oscillation, there is a sustaining 8-yr variation in Area2 (Figure 9e).

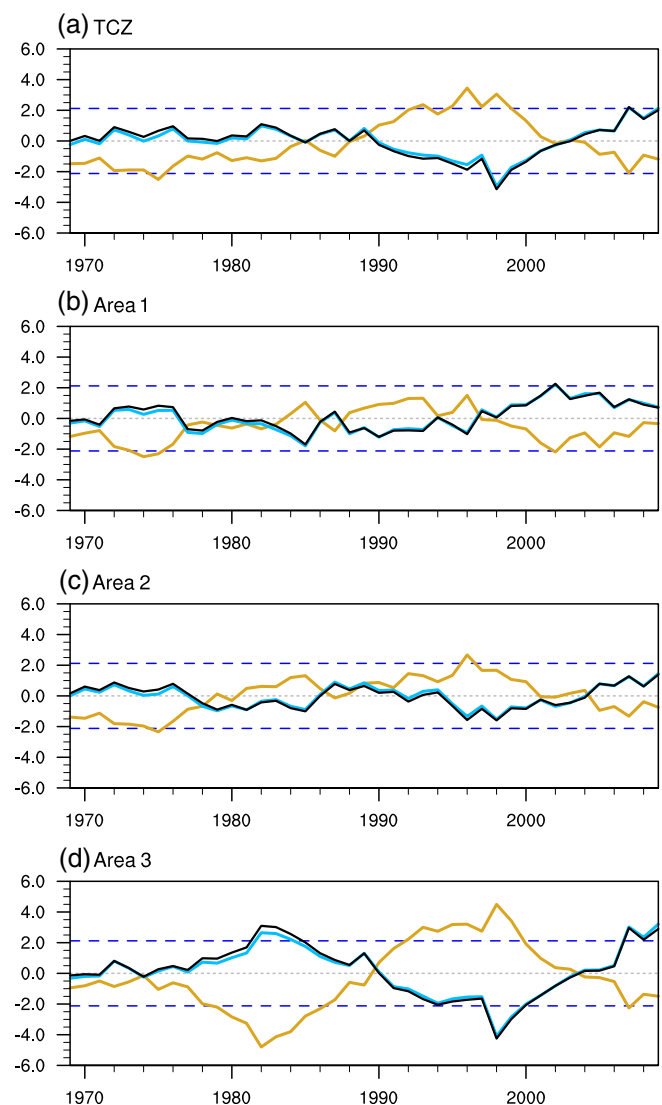


FIGURE 8 Moving *t* test (step = 9) of summer PET (yellow solid line) and PRE (blue solid line) as well as SM_AI (black solid line) for the whole TCZ (a) and its three subregions during 1961–2018. Blue dashed line indicated the significant level of .05 [Colour figure can be viewed at wileyonlinelibrary.com]

Compared with the other two subregions, the wavelet power energy of SM_AI in Area3 is very concentrated, showing strong oscillations of 3–8 years during

1990–2010 (Figure 9g). A forceful multidecadal oscillation of a 28-year period across the whole study period is detected outside of the cone of influence, which is the

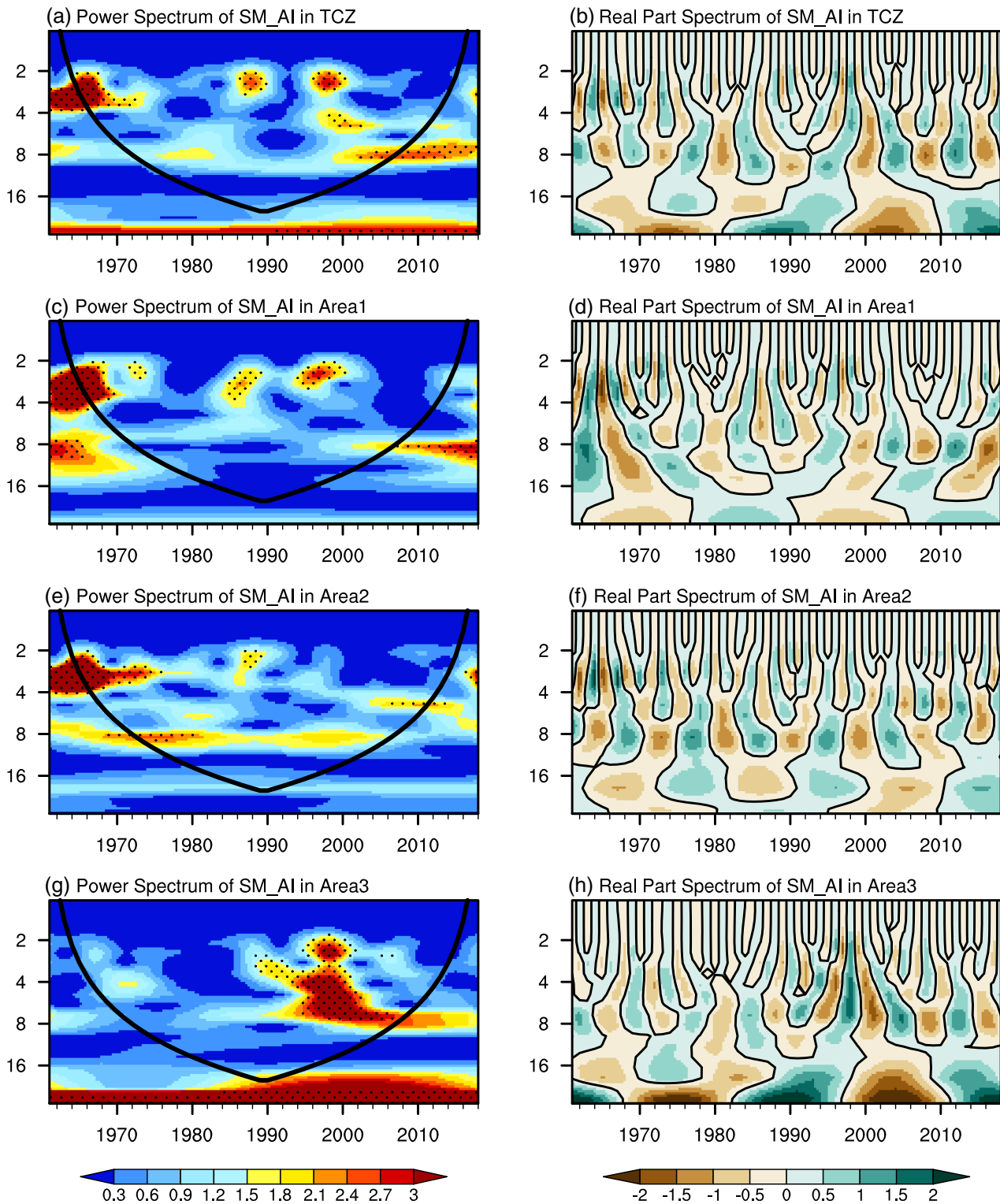


FIGURE 9 (a), (c), (e) and (g) The wavelet power spectrum and (b), (d), (f) and (h) real part spectrum of SM_AI in TCZ and its three subregions using the Morlet wavelet. Dots indicates time-periodicity regions with significant concentrations of spectral power ($\text{sig} = .05$) [Colour figure can be viewed at wileyonlinelibrary.com]

main source of the interdecadal oscillation background field of the whole TCZ. According to its real part spectrum, there are uniformed strong positive (wet) and negative (dry) signals at all scales around 1998, with the zero line nearly vertical, implying an intense drought process (Figure 9h). Based on the analysis above, we can come to conclusion that the drying of TCZ in the late 90s mainly happened in its northeast subregion.

5 | MONSOON RAINY SEASON AND ITS INFLUENCE ON TCZ

As noted in Section 2.3, we defined MRO, MRR, and MRD to quantitatively describe the impact of summer monsoon on the onset, retreat, and duration of the rainy season over TCZ. Since the southern boundary of TCZ is extraordinarily tortuous and complex annually, we simplify the southern edge and split it into five segments(-Figure 10): 100–105 °E, 37°N; 105–110 °E, 36°N; 110–115

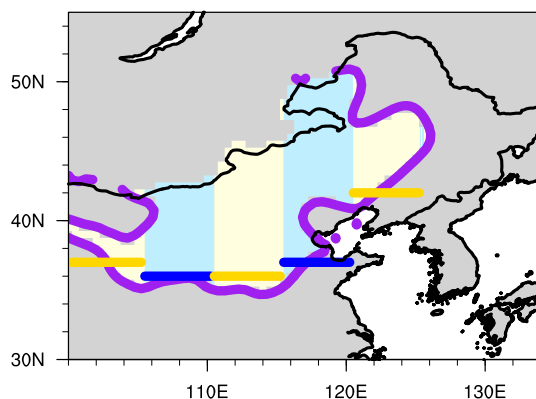


FIGURE 10 Boundaries of TCZ (thick purple lines) and simplified five segments of TCZ southern boundary (yellow or blue lines) and their corresponding affected areas(contour) [Colour figure can be viewed at wileyonlinelibrary.com]

°E, 36°N; 115–120 °E, 37 N; 120–125 °E, 42°N. Then, the latitudinal average of precipitation is used to define MRO, MRR and MRD of relevant regions according to Section 2.3. The filtered precipitation does not always exceed 4 mm during May to September, so there is missing data in MRO and MRR which means the corresponding area is not influenced by monsoon rainy season that year. Table 1 shows the amount of years influenced by monsoon rainy season and statistical mean and variance of MRO, MRR and MED. Frequency distributions in different longitude range of TCZ are portrayed as box plots in Figure 11, and the time series are illustrated in Figure 12.

Generally, monsoon rainy season usually begins in late June to early July and ends in mid to late August, lasting about 1 or 2 months, depending on different regions. Monsoon rainy season of 100–105°E longitude range in TCZ begins in mid-July, ends in mid-August, and the average duration of rainy season lasts less than a month. Compared with other segments, MRD here is much shorter, and it has more years without penetration of the summer monsoon (Table 1). MRO and MRR in 110–115°E are in early July and late August, respectively, and MRD is about 54 days. Rainy season of the other three segments all start from the end of June, end at the end of August, lasting about 2 months. It is noteworthy that MRO, MRR and MRD of all segments have a large degree of dispersion (Figure 11). The distributions of three indexes of 115–120°E were comparatively centralized.

It is evident that MRD is significantly correlated with MRO and MRR because of its definition. However, the relationship between MRO and MRR is quite different. There is a good correlation between MRO and MRR of the western two segments of the southern boundary of TCZ, with the correlation coefficients of 0.32 and 0.36, respectively, which passed the significance test of 0.05, while there is no obvious correlation between the onset

TABLE 1 The number of influenced years of five segments of TCZ southern boundary and the mean and standard deviation of MRO, MRR and MRD during 1961–2018

		100–105E, 37 N	105–110E, 36 N	110–115E, 36 N	115–120E, 37 N	120–125E, 42 N
Influenced years		47	54	57	56	57
MRO	Mean (JD)	197	187	174	173	171
	SD (JD)	21.8	27.1	23.7	21.9	25.0
MRR	Mean (JD)	229	244	239	238	231
	SD (JD)	19.6	27.7	25.2	16.1	20.3
MRD	Mean (day)	27.2	54	65	63	60
	SD (day)	25.5	33.3	36.5	30.7	29.9

and retreat dates in other three eastern segments (Figure 12).

To illuminate how the AI and precipitation response to the summer monsoon, we conducted a linear regression analysis of MRD, MRO and MRR against corresponding summer precipitation and SM_AI in TCZ as shown in Figure 13 and Figure 14. MRO in all five segments except 105–110°E are significantly negatively correlated to precipitation and SM_AI, and the correlation coefficient (r) varied from -0.32 to -0.25 and -0.31 to -0.26 , respectively, with a significant level of 0.1. MRR in

all five segments except 115–120°E are significantly positively correlated to precipitation and SM_AI, and the correlation coefficient (r) varied from 0.27 to 0.35 and 0.25 to 0.31. In comparative terms, MRD in all longitude ranges

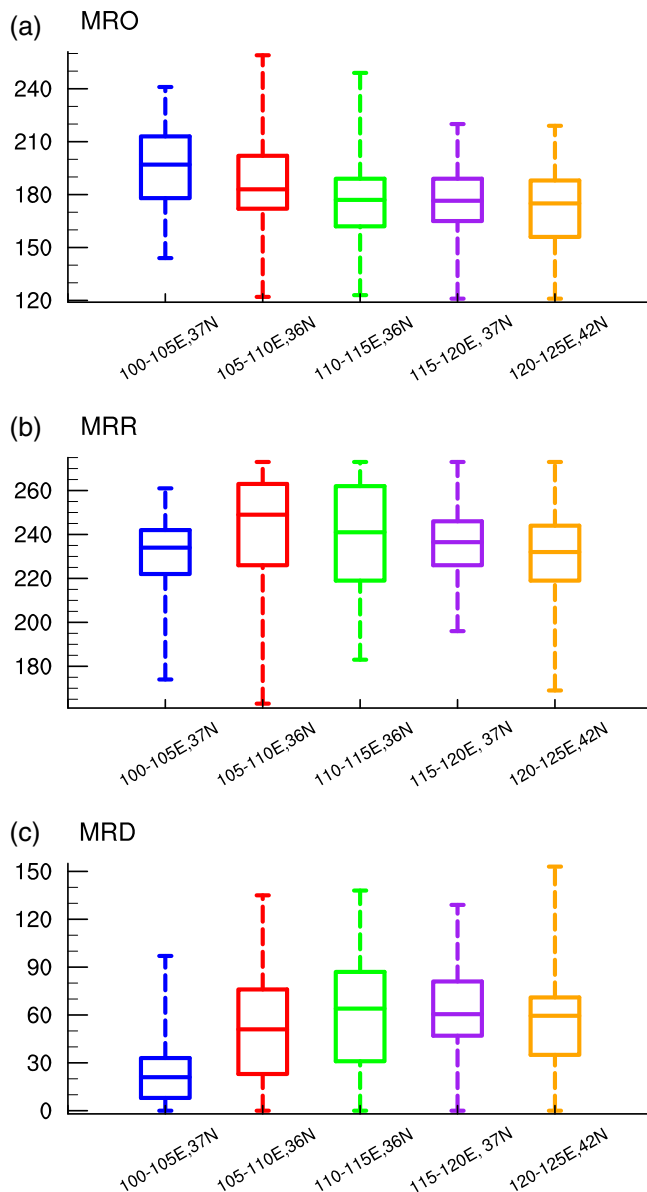


FIGURE 11 Box plots of MRO (Julian Day), MRR (Julian Day) and MRD (days) of different part of TCZ. Boxes encompass the central of 50%, lines encompass all the values [Colour figure can be viewed at wileyonlinelibrary.com]

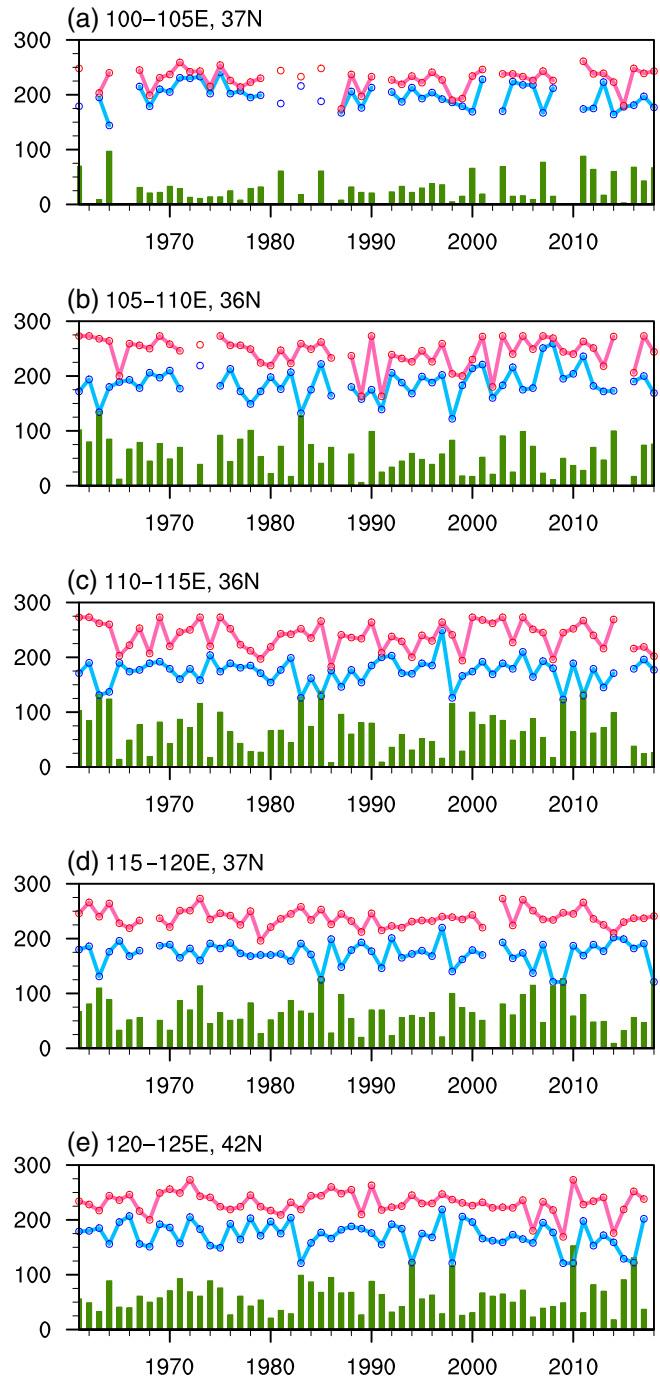


FIGURE 12 Time series of the time summer monsoon influenced TCZ during 1961–2018. Pink line with circle is the date monsoon rainy season begins (MRO, unit: Julian Day), and the blue one represents the day it ends (MRR, unit: Julian Day). The green bar is the rainy season duration (MRD, unit: Day) [Colour figure can be viewed at wileyonlinelibrary.com]

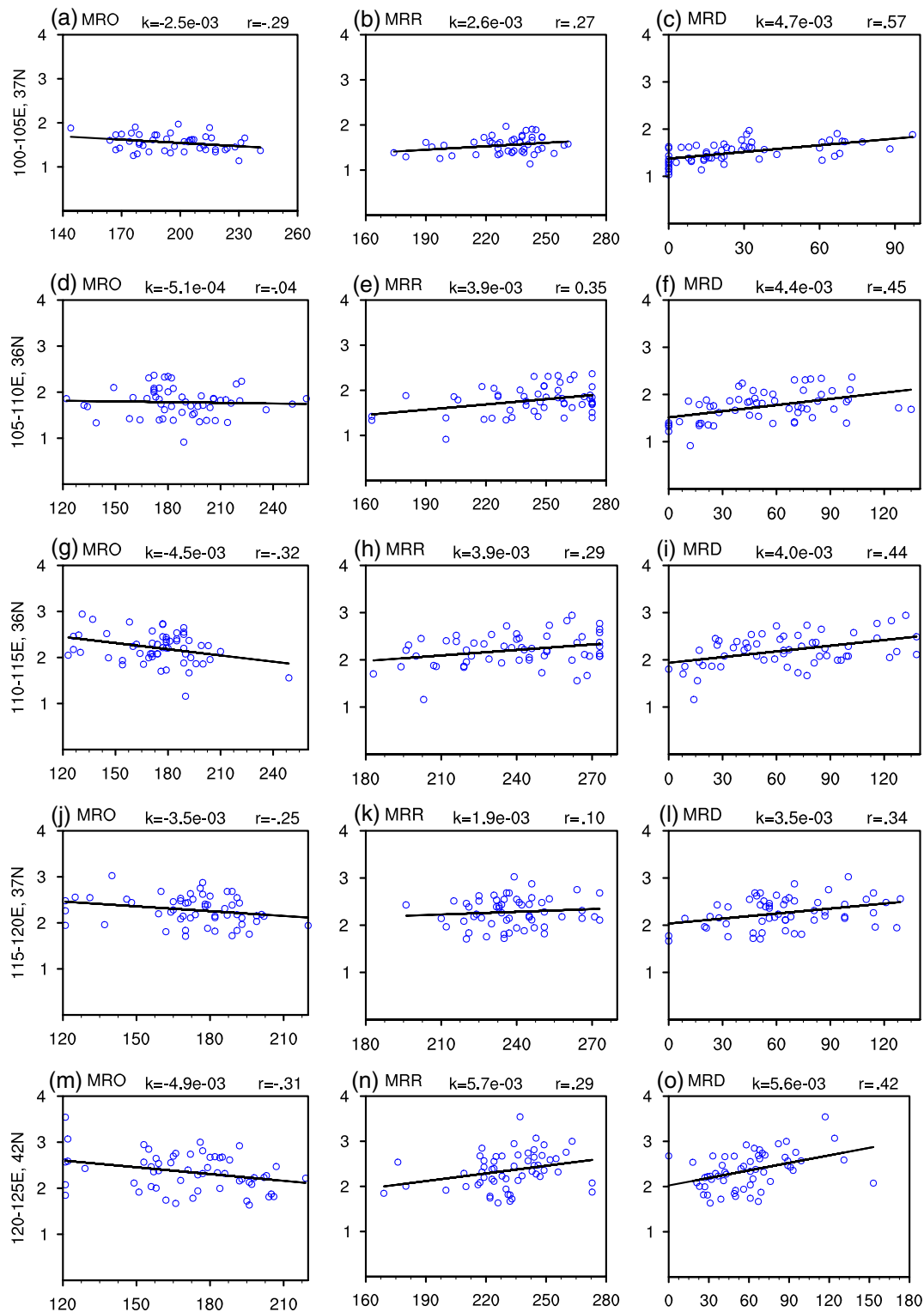


FIGURE 13 Scatter plot of summer precipitation versus MRO (first column), MRR (second column) and MRD (third column) of five segments (first to fifth row) of TCZ southern boundary, with linear regression line superimposed (black line). The Y-axis is area average summer rainfall (units, mm/day) and X-axis represents MRO, MRR or MRD. The values of k and r are the regression and correlation coefficients, respectively. All passed significant level of .1 except k and r values in (d) and (k) [Colour figure can be viewed at wileyonlinelibrary.com]

shows stronger correlations with precipitation and SM_AI with r of 0.34–0.57 and 0.33–0.54. The strongest correlations between MRD and precipitation existed in

100–105°E, although monsoon rainy season lasted the shortest in this area. It seems like the west region of TCZ is more sensitive to the monsoon. However, the time series

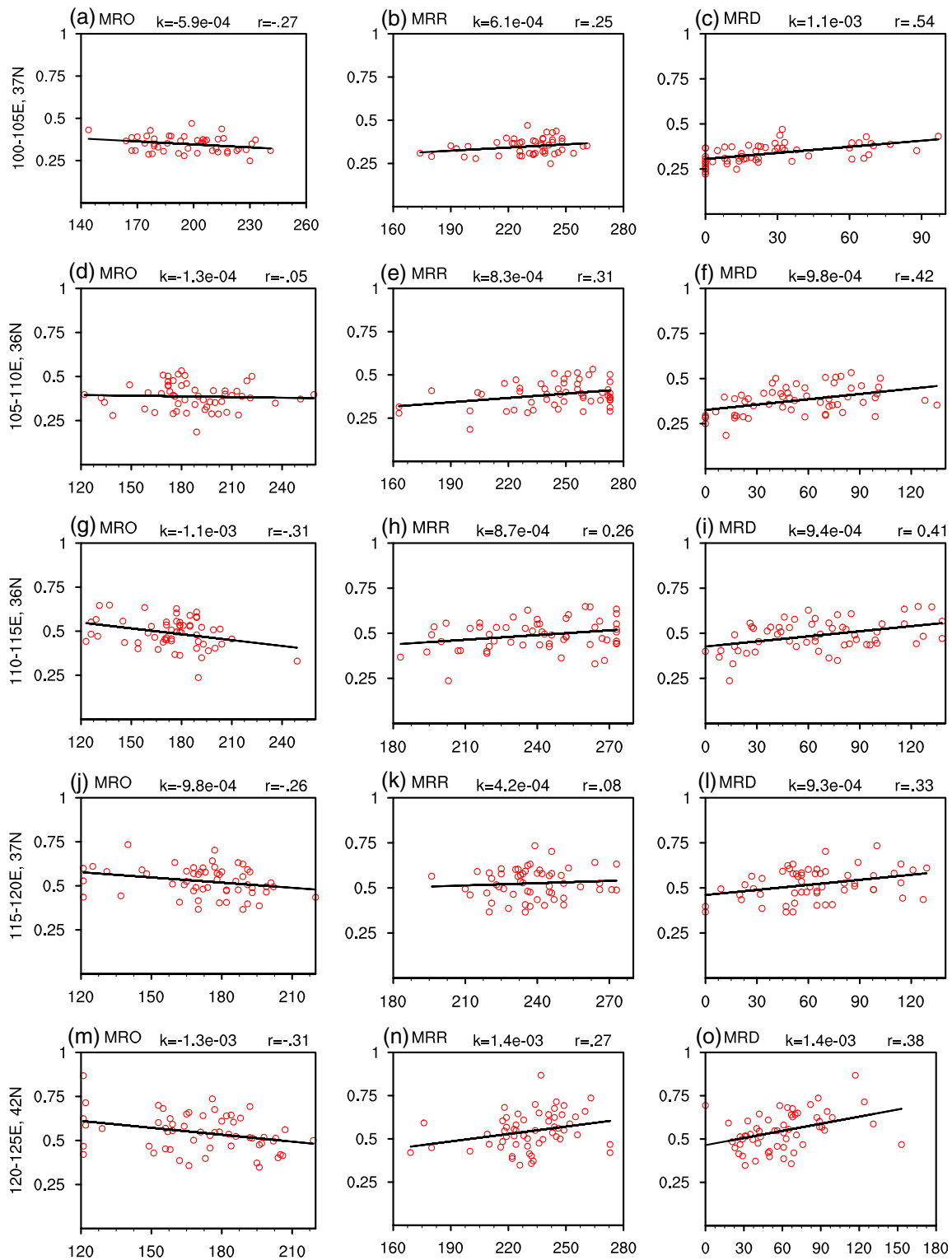


FIGURE 14 Same as Figure 13 except for SM_AI. All passed significant level of .1 except k and r values in (d) and (k) [Colour figure can be viewed at wileyonlinelibrary.com]

of MRD shows no dramatic decrease in 120–125°E in late 1990s (Figure 12e), while there is a significant shift toward drier conditions in the same period in northeast subregion

(Figure 7d). It is probably because MRD can only indicate how long monsoon rainy lasts, yet precipitation intensity also plays an important part in total summer precipitation.

6 | CONCLUSIONS AND DISCUSSION

TCZ was mainly characterized by the semi-arid climate, with a large gradient of precipitation and SM_AI in summer. Due to little change of summer potential evaporation, Summer AI in TCZ is mainly determined by precipitation, showing little significant long-term trend since 1961.

Global consistent change in TCZ is identified in the first mode of EOF analysis of SM_AI during the past 60 years, with a clear dry process in the late 1990s to the beginning of the 20th century. The second mode depicted positive (southwest) – negative (northeast) departures, while the third mode revealed a “– + –” meridional pattern. Although this article is centered on the spatio-temporal variation manners, a simple investigation on dynamics of the first two modes are made for better understanding how EASM and mid-latitude system affect TCZ. Since the annual components explains the majority of the variance of PCs, Figure 15 shows the anomalous patterns of vertically integrated summer precipitable water, wind and geopotential height anomaly at 700 hPa regressed onto interannual components of PC1 and PC2. The interannual variation of first mode is mainly influenced by EASM circulation (Figure 15a), since the southwesterlies bring a lot of moisture from northwest Pacific sea in the positive phase. Meanwhile, the low pressure anomaly over Mongolian area also contribute to the convergence of water content by strengthened west wind. The second mode (Figure 15b) is likely to be exclusively affected by the mid-latitude systems. It can be seen that the positive phase features an abnormal low pressure center in Northeast China with an associated cyclonic flow around it. Such pattern produced north wind anomalies preventing moisture penetration into the southwest part of TCZ, while the low pressure in the northeast part of TCZ is favourable for the up-motion and convection activities.

TCZ can be divided into three subregions from south to north, based on REOF results. Area1(the southernmost part of TCZ) had the largest interannual fluctuation, only one abrupt changepoint of decadal variation in 2002 (dry to wet) was detected in this subregion. Compared with the other two subregions, the northwest area (Area 2) was relatively steady. The most significant decadal variability was observed in the northeast (Area 3), with three decadal abrupt points detected:1982 (dry–wet), 1998 (wet–dry) and 2007 (dry–wet). According to the wavelet analysis results, the distinguished drying process in TCZ in the late 1990s, which mainly happened in the northeast subregion, is the result of interannual change and interdecadal oscillation.

Monsoon rainy season indicators-MRO, MRR and MRD, influence dry-wet conditions in TCZ by controlling monsoon rainfall. It begins in late June to early July, ends in late August to early September, lasting about 1 or 2 months depending on different longitude range. We noticed an early monsoon onset date does not necessarily mean an early retreat date. Only the west part of TCZ (100–110°E) has a significant correlation between MRO and MRR. Although the duration of monsoon rainy season is significant related to summer wet and dry conditions in TCZ compared with MRO and MRR, the importance of precipitation intensity should also be taken into account. Noted that even though the westmost part of TCZ (100–105°E) is characterized by fewer influenced years and shorter duration, it is more sensitive to monsoon activity than other parts.

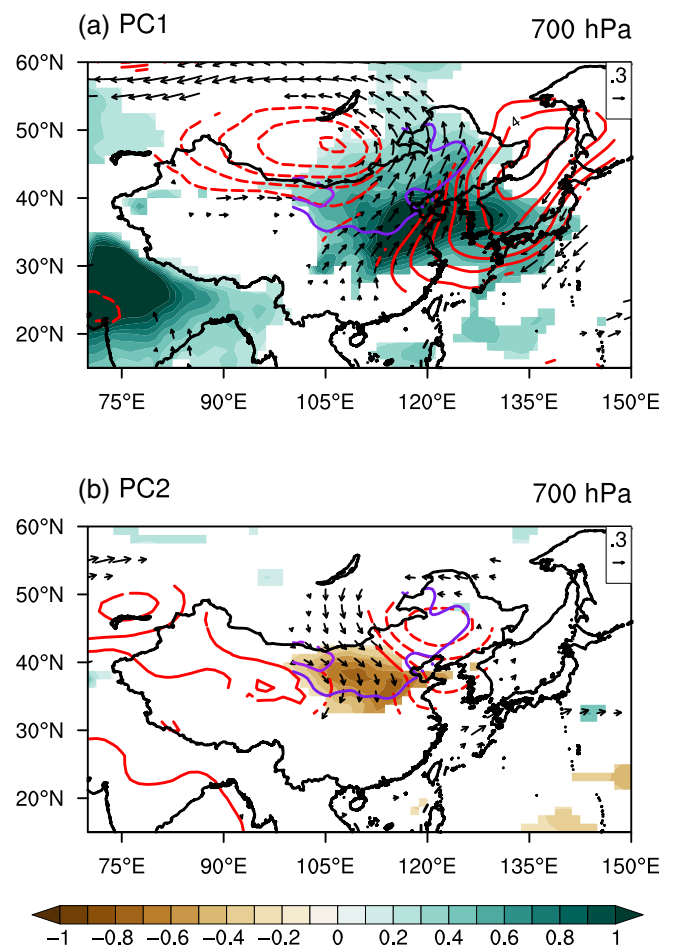


FIGURE 15 The regressed precipitable water (shading, unit: $\text{kg}\cdot\text{m}^{-2}$), wind (vector, unit: $\text{m}\cdot\text{s}^{-1}$) and geopotential height anomaly (line, unit: gpm) at 700 hPa based on the annual components of PC1 (a) and PC2 (b) during 1961–2018. The dashed red line indicates low abnormal pressure while the solid red line indicates the high abnormal pressure. Results above the 95% confidence level are marked [Colour figure can be viewed at wileyonlinelibrary.com]

ACKNOWLEDGEMENT

Prof Gang Huang contributed equally as co-corresponding author (E-mail: hg@mail.iap.ac.cn). We thank two anonymous reviewers for their constructive suggestions and comments, which led to a significant improvement in the paper. This work was supported by the National Natural Science Foundation of China Grant Nos. 41875115, 41961144016, 41831175 and 41530425, and the Key Deployment Project of Centre for Ocean Mega-Research of Science, Chinese Academy of Science (COMS2019Q03).

ORCID

Qiulin Wang  <https://orcid.org/0000-0001-9113-4546>

Lin Wang  <https://orcid.org/0000-0002-3810-4724>

Gang Huang  <https://orcid.org/0000-0002-8692-7856>

REFERENCES

- Chen, H. and Sun, J. (2015) Changes in drought characteristics over China using the standardized precipitation evapotranspiration index. *Journal of Climate*, 28, 5430–5447.
- Chen, J., Huang, W., Jin, L., Chen, J., Chen, S. and Chen, F. (2018) A climatological northern boundary index for the east Asian summer monsoon and its interannual variability. *Science China Earth Sciences*, 61, 13–22.
- Chen, W., Wang, L., Feng, J., Wen, Z.P., Ma, T.J., Yang, X.Q. and Wang, C.H. (2019) Recent Progress in studies of the variabilities and mechanisms of the east Asian monsoon in a changing climate. *Advances in Atmospheric Sciences*, 36, 887–901.
- Fei, H., Liang, L.D., Xu, T., Shigong, W. and Hui, W. (2009) Determination on the North boundary of summer monsoon in east Asian with soaking rainfall. *Journal of Applied Meteorological Science*, 20, 530–538.
- Fu. (1992) Transitional climate zones and biome boundaries: a case study from China. In: Hansen, A.J. and Castri, F.D. (Eds.) *Land-scape Boundaries*. New York: Springer-Verlag, pp. 394–402.
- Harada, Y., Kamahori, H., Kobayashi, C., Endo, H., Kobayashi, S., Ota, Y., Onoda, H., Onogi, K., Miyaoka, K. and Takahashi, K. (2016) The JRA-55 reanalysis: representation of atmospheric circulation and climate variability. *Journal of the Meteorological Society of Japan*, 94, 269–302.
- Hargreaves, G.H. and Samani, Z.A. (1985) Reference crop evapotranspiration from temperature. *American society of Agricultural Engineer*, 1, 85–97.
- Huang, J., Guan, X. and Ji, F. (2012a) Enhanced cold-season warming in semi-arid regions. *Atmospheric Chemistry and Physics*, 12, 5391–5398.
- Huang, J., Li, Y., Fu, C., Chen, F., Fu, Q., Dai, A., Shinoda, M., Ma, Z., Guo, W., Li, Z., Zhang, L., Liu, Y., Yu, H., He, Y., Xie, Y., Guan, X., Ji, M., Lin, L., Wang, S., Yan, H. and Wang, G. (2017) Dryland climate change: recent progress and challenges. *Reviews of Geophysics*, 55, 719–778.
- Huang, J., Ma, J., Guan, X., Li, Y. and HE, Y. (2019) Progress in semi-arid climate change studies in China. *Advances in Atmospheric Sciences*, 36, 922–937.
- Huang, R., Liu, Y. and Feng, T. (2012b) Interdecadal change of summer precipitation over eastern China around the late-1990s and associated circulation anomalies, internal dynamical causes. *Chinese Science Bulletin*, 58, 1339–1349.
- Kobayashi, S., Ota, Y., Harada, Y., Ebata, A., Moriwa, M., Onoda, H., Onogi, K., Kamahori, H., Kobayashi, C., Endo, H., Miyaoka, K. and Takahashi, K. (2015) The JRA-55 reanalysis: general specifications and basic characteristics. *Journal of the Meteorological Society of Japan*, 93, 5–48.
- Li, C.Y. and Zhou, W. (2014) Interdecadal change in South China Sea tropical cyclone frequency in association with zonal sea surface temperature gradient. *Journal of Climate*, 27, 5468–5480.
- Li, C.Y. and Zhou, W. (2015) Multiscale control of summertime persistent heavy precipitation events over South China in association with synoptic, intraseasonal, and low-frequency background. *Climate Dynamics*, 45, 1043–1057.
- Li, C.Y., Zhou, W. and Li, T. (2014) Influences of the Pacific-Japan teleconnection pattern on synoptic-scale variability in the western North Pacific. *Journal of Climate*, 27, 140–154.
- Li, X.Z., Zhou, W. and Chen, Y.Q. (2015b) Assessment of regional drought trend and risk over China: a drought climate division perspective. *Journal of Climate*, 28(18), 7025–7037.
- Li, Y., Huang, J.P., Ji, M.X. and Ran, J.J. (2015a) Dryland expansion in northern China from 1948 to 2008. *Advances in Atmospheric Sciences*, 32, 870–876.
- Lu, W. and Jia, G.S. (2013) Fluctuation of farming-pastoral ecotone in association with changing East Asia monsoon climate. *Climatic Change*, 119, 747–760.
- North, G.R., Bell, T.L., Cahalan, R.F. and Moeng, F.J. (1982) Sampling errors in the estimation of empirical orthogonal functions. *Monthly Weather Review*, 110, 699–706.
- Ou, T.H. and Qian, W.H. (2006) Vegetation variations along the monsoon boundary zone in East Asia. *The Chinese Journal of Geophysics (in Chinese)*, 49, 698–705.
- Piao, J., Chen, W., Wei, K., Liu, Y., Graf, H.-F., Ahn, J.-B. and Pogoreltsev, A. (2017) An abrupt rainfall decrease over the Asian inland plateau region around 1999 and the possible underlying mechanism. *Advances in Atmospheric Sciences*, 34, 456–468.
- Qian, C., Yan, Z. and Fu, C. (2011) The role of changes in the annual cycle in earlier onset of climatic spring in northern China. *Advances in Atmospheric Sciences*, 28, 284–296.
- Qian, W.H., Ding, T., Hu, H., Lin, X. and Qin, A. (2009) An overview of dry-wet climate variability among monsoon-westerly regions and the monsoon northernmost marginal active zone in China. *Advances in Atmospheric Sciences*, 26, 630–641.
- Qian, W.H., Lin, X., Zhu, Y.F., Xu, Y. and Fu, J.L. (2007) Climatic regime shift and decadal anomalous events in China. *Climatic Change*, 84, 167–189.
- Qian, W.H. and Qin, A. (2007) Precipitation division and climate shift in China from 1960 to 2000. *Theoretical and Applied Climatology*, 93, 1–17.
- Shi, Z.T., Zhang, L.Y. and Sui, G. (1994) Natural disasters and their formation causes on Chinese monsoon marginal belt. *Journal of Catastrophology (in Chinese)*, 9, 59–64.
- Torrence, C. and Compo, G.P. (1998) A practical guide to wavelet analysis. *Bulletin of the American Meteorological Society*, 79, 61–78.
- Wang, Bing and Lin Ho. (2002) Rainy season of the Asian-Pacific summer monsoon. *Journal of Climate*, 15, 386–398.

- Wang, H. and Li, D.L. (2011) Correlation of surface sensible heat flux in the arid region of northwestern China with the northern boundary of the east Asian summer monsoon and Chinese summer precipitation. *Journal of Geophysical Research-Atmospheres*, 116, 1441–1458.
- Wang, L., Chen, W., Huang, G. and Zeng, G. (2017) Changes of the transitional climate zone in East Asia: past and future. *Climate Dynamics*, 49, 1463–1477.
- Wang, W.W., Zhou, W. and Chen, D.L. (2014) Summer high temperature extremes in Southeast China: bonding with the El Niño-southern oscillation and east Asian summer monsoon coupled system. *Journal of Climate*, 27, 4122–4138.
- Wang, W.W., Zhou, W., Wang, X., Fong, S.K. and Leung, K.C. (2013) Summer high temperature extremes in Southeast China associated with the east Asian jet stream and circumglobal teleconnection. *Journal of Geophysical Research*, 118, 8306–8319.
- Xu, Y., Zhao, P., Si, D., Cao, L., Wu, X., Zhao, Y. and Liu, N. (2019) Development and preliminary application of a gridded surface air temperature homogenized dataset for China. *Theoretical and Applied Climatology*, 139, 505–516. <https://doi.org/10.1007/s00704-019-02972-z>.
- Xu, Z., Fan, K. and Wang, H. (2015) Decadal variation of summer precipitation over China and associated atmospheric circulation after the late 1990s. *Journal of Climate*, 28, 4086–4106.
- Zeng, X.B. and Lu, E. (2004) Globally unified monsoon onset and retreat indexes. *Journal of Climate*, 17, 2241–2248.
- Zhang, Lixia and Zhou, Tianjun (2015) Drought over East Asia: a review. *Journal of Climate*, 28, 3375–3399.
- Zhao, W., Chen, W., Chen, S., Nath, D. and Wang, L. (2020) Interdecadal change in the impact of North Atlantic SST on august rainfall over the monsoon transitional belt in China around the late 1990s. *Theoretical and Applied Climatology*, 140, 503–516. <https://doi.org/10.1007/s00704-020-03102-w>.
- Zhao, W., Chen, W., Chen, S., Yao, S.-L. and Nath, D. (2019) Interannual variations of precipitation over the monsoon transitional zone in China during August-September: role of sea surface temperature anomalies over the tropical Pacific and North Atlantic. *Atmospheric Science Letters*, 20(1), e872.

How to cite this article: Wang Q, Wang L, Huang G, Piao J, Chotamonsak C. Temporal and spatial variation of the transitional climate zone in summer during 1961–2018. *Int J Climatol*. 2021;41: 1633–1648. <https://doi.org/10.1002/joc.6902>